

Pseudocapacitance Properties of Co₃O₄ Nanoparticles Synthesized Using a Modified Sol-Gel Method

Michele Karoline Lima-Tenório^a, Carlos Sergio Ferreira^b, Querem Hapuque Felix Rebelo^b, Rodrigo Fernando Brambilla de Souza^b, Raimundo Ribeiro Passos^b, Edgardo Alfonso Gómes Pineda^a, Leandro Aparecido Pocrifka^{b*}

^a Departamento de Química, Maringá, Universidade Estadual de Maringá, PR, Brazil

^b Departamento de Química, Universidade Federal do Amazonas, Manaus, AM, Brazil

Received: May 25, 2017; Revised: December 14, 2017; Accepted: December 30, 2017

This work reports the synthesization of nanoparticles cobalt oxide (Co₃O₄) with no secondary phase by a modified sol-gel method and its structural morphological and electrochemical characterizations. FTIR, XRD and Raman analysis showed the formation of spinel cobalt oxide with no secondary phase. TEM images revealed that an undefined morphology with average crystallite size estimated by Scherrer's equation was found to be 30 nm. Experiments of cyclic voltametric, galvanostatic charge-discharge and impedance spectroscopy were evaluated at 1 mol L⁻¹ KOH and revealed an intrinsic pseudocapacitance. The studies of complex capacitance and complex power revealed the resistive and capacitive characteristics with a specific capacitance of 120 F g⁻¹.

Keywords: Adapted Sol-gel Method, Co₃O₄ nanoparticles, pseudocapacitance, complex capacitance, complex power.

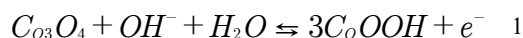
1. Introduction

Synthesis of nanoparticles semiconductor materials with different sizes and shapes are considered an attractive field of research¹. Physical and chemical properties such as high surface area, volume and high interfacial reactivity, make nanoparticles attractive in various fields of applications: catalysis², magnetic materials³, sensors⁴ and energy storage like batteries⁵ and electrochemical capacitors⁶.

When the nanomaterial is used for the purpose of energy storage, it can be done in two ways, directly and indirectly. In the direct form, the materials are constituted with porous materials of large surface areas that allow the storage of electric charges by electrostatic adsorption on the surface and pores^{7,8}. In an indirect way, the material storage by quick faradaic reactions at the electrode/electrolyte interface by a mechanism known as pseudocapacitance⁹. Indirect storage is possible in materials such as conductive polymers and oxides of transition metals. In metallic oxides, the pseudocapacitance can be classified as intrinsic or extrinsic^{10,11}. Intrinsic pseudocapacitance can charge storage for a wide range of particle sizes and morphologies. The main oxides studied are RuO₂¹², MnO₂¹³, NiO¹⁴, Fe₃O₄¹⁵ e Co₃O₄¹⁶.

Cobalt oxide is a semiconductor p-type that can exist in three different forms (CoO, Co₂O₃ and Co₃O₄), is naturally abundant and environmentally safe¹⁷ besides excellent redox

activity and low cost compared to other transition metal oxides, such as ruthenium¹⁸. Particularly as electrodes, in Co₃O₄ (cobaltic oxide) form, cobalt oxide exhibits good electrochemical performance in alkaline solution, and faradaic redox processes occurring at the surface can be described according to the reactions¹⁹ 1 and 2:



Controlled synthesis of Co₃O₄ nanostructures applied on pseudocapacitive energy storage are studied by different synthesis methodologies. For instance, Shinde *et al.* prepared Co₃O₄ thin films by the spray pyrolysis technique and obtained a specific capacitance of 74 F g⁻¹¹⁸. By the microwave method Yan *et al.* prepared a composite of Co₃O₄ and graphene nanosheet (GNS)/Co₃O₄ that presented a specific capacitance of 243 F g⁻¹²⁰. Using a hydrothermal method Wang *et al.* obtained Co₃O₄ nanorods with a value of 280 F g⁻¹²¹. Plasma spray route was used for Tummala *et al.* to obtain electrodes films with specific capacitance of 166 F g⁻¹²². The conventional sol-gel method^{23,24,25,26,27} has some advantages like high purity and form homogeneous

*e-mail: pocrifka@gmail.com

products with different morphologies and has been employed in obtaining nanostructures of oxides for the purpose of energy storage^{28,29,30}. On the other hand, it uses organic solvents, expensive reagents and the control of pH and temperature are also necessary and generally more than one phase of cobalt oxide is produced together^{31,32,33}

This work reports the synthesis of Co_3O_4 nanopowder by an adapted sol-gel method, previously published by our research group³⁴. The oxide obtained was characterized physically by techniques of infrared spectroscopy, X-ray diffraction, Raman spectroscopy and transmission electron microscopy. The electrochemical characterization was used to evaluate the capacitive characteristics of the energy storage through techniques of the cyclic voltammetry, galvanostatic charge/discharge and electrochemical impedance spectroscopy in KOH electrolyte that was studied for the concentration of 1 mol L^{-1} .

2. Experimental

Poly(vinyl alcohol) (PVA, 87 - 89 wt.%) hydrolyzed and MW 146,000 - 186,000 were purchased from Aldrich. $\text{Co}(\text{NO}_3)_2 \cdot 6\text{H}_2\text{O}$ (98 wt.% Synth). The cobalt oxide nanoparticles were synthesized by an adapted sol-gel method. Aqueous diluted PVA (10% w/v) and saturated metal nitrate solutions were prepared separately and then mixed at Co^{2+} : PVA monomeric unit ratio of 1:6. The solution was kept at room temperature under stirring for 2 h and then heated under vigorous stirring (approximately 250°C), until total water evaporation and partial thermal degradation of the polymer. The nanoparticles material was achieved after calcination of the obtained powder under atmospheric air at 400°C .

The cobalt oxide powder was characterized by infrared spectroscopy (FTIR) using FTIR-BOMEM-100 Spectrometer with KBr pellet. The crystalline phase was identified by X-ray diffraction (XRD) using Shimadzu XRD-6000X-ray diffractometer with monochromated Cu-K α radiation ($\lambda = 1.5406 \text{ \AA}$). Reflection X-ray powder diffraction data were obtained in the following conditions: $2\theta = 10 - 80^\circ$, 40 kV, 30 mA, scan rate of 2 min^{-1} and slit width of 0.30 mm.

Raman measurement was carried out using Bruker Senterra Raman microscope with 785 nm laser radiation and laser power of 25 mW. The spectra were acquired by averaging hundred acquisitions of 3 s with $a \times 20$ objective. The obtained cobalt oxide morphology was analyzed using 120 kV JEOL JEM-1400 transmission electron microscope (TEM) with a Carl Zeiss EM10 microscope operating at 80 KV.

Cyclic voltammograms, chronoamperometric and electrochemical impedance experiments were carried out in a conventional three-electrode cell using Autolab Potentiostat (PGSTAT 302N). The cobalt oxide powder prepared by a homogeneous mixture of Co_3O_4 nanoparticles (85 wt%), activated carbon (10 wt%) and polytetrafluorethylene (PTFE, 5 wt%)³⁵ was deposited onto a titanium substrate and

used as working electrode, Ag/AgCl/saturated KCl electrode was used as a reference electrode and a KOH solution as electrolyte. Cyclic voltammograms were recorded at scan rates of 1, 10 and 25 mV s^{-1} in the potential range of 0 - 0.6 V, at room temperature. Charge/discharge tests were recorded for current densities of 1, 3 and 5 mA cm^{-2} in the same potential range of voltammograms. Electrochemical impedance measurements were conducted in 0.4 V with the aid of a frequency response analyzer module coupled to the model AUTOLAB FRA. After 300 s polarization, spectra were obtained in the frequency range of 10 mHz to 10 kHz, to which an alternating disturbance 10mV peak to peak was applied.

3. Results and Discussion

The cobalt oxide as obtained was analyzed by FTIR spectroscopy and its spectrum is depicted in Fig. 1a. Two absorption bands centered at 651 cm^{-1} and 565 cm^{-1} are assigned to the fingerprint stretching vibrations of Co-O bond³⁶. The band at 565 cm^{-1} is related to Co-O vibrations in the octahedral site, whereas the band at 651 cm^{-1} is associated to Co-O vibrations in the tetrahedral site of the lattice, indicating the formation of pure phase of Co_3O_4 ³⁷. The presence of these bands in the lower wavenumber region suggests that the materials were finely crystallized in the nano range³⁸.

X-ray diffraction pattern of cobalt oxide nanoparticles produced with refinement by the Rietveld method performed using the GSAS-EXPGUI software package is presented in Fig. 1b. And it is possible to see peaks at $\approx 19^\circ, 32^\circ, 36^\circ, 39^\circ, 45^\circ, 56^\circ, 59^\circ, 66^\circ, 74^\circ, 77^\circ$ and 78° referent to (111), (220), (311), (222), (400), (422), (333), (440), (620), (533) and (622) planes, corresponding to Co_3O_4 . The obtained lattice parameters, with Rietveld method, were $a = b = c = 0.8091 \text{ nm}$, with a satisfactory agreement with ICSD # 9362 ($a = b = c = 0.8065 \text{ nm}$)³⁹, corresponding to a single phase of spinel structure, indicating nanoparticles in the Co_3O_4 compound. The average size of crystallites calculated by Scherrer's equation was obtained with approximately 30 nm, caused by the reduced crystallite size and the crystalline lattice distortion. All the diffraction peaks could be well indexed to spinel Co_3O_4 phase (JCPDS 42-1467).

Raman spectrum of the synthesized nanoparticle material is depicted in Fig. 1c. It has clearly displayed five well-defined peaks located at approximately 194, 478, 518, 616 and 686 cm^{-1} , which correspond, respectively to the A_{1g} , F_{2g}^2 , F_{2g}^1 , E_g and F_{2g}^3 modes of Co_3O_4 crystalline, in agreement with the group theory⁴⁰. When compared with the Raman-active phonon modes of Co_3O_4 , these peaks show a red-shift⁴¹. This phenomenon is attributed to the optical phonon confinement effect in nanoparticles that can cause uncertainty in the phonon wave vectors and then a downshift of the Raman peaks⁴². These results are consistent with the result of Co_3O_4 nanoparticles for XRD.

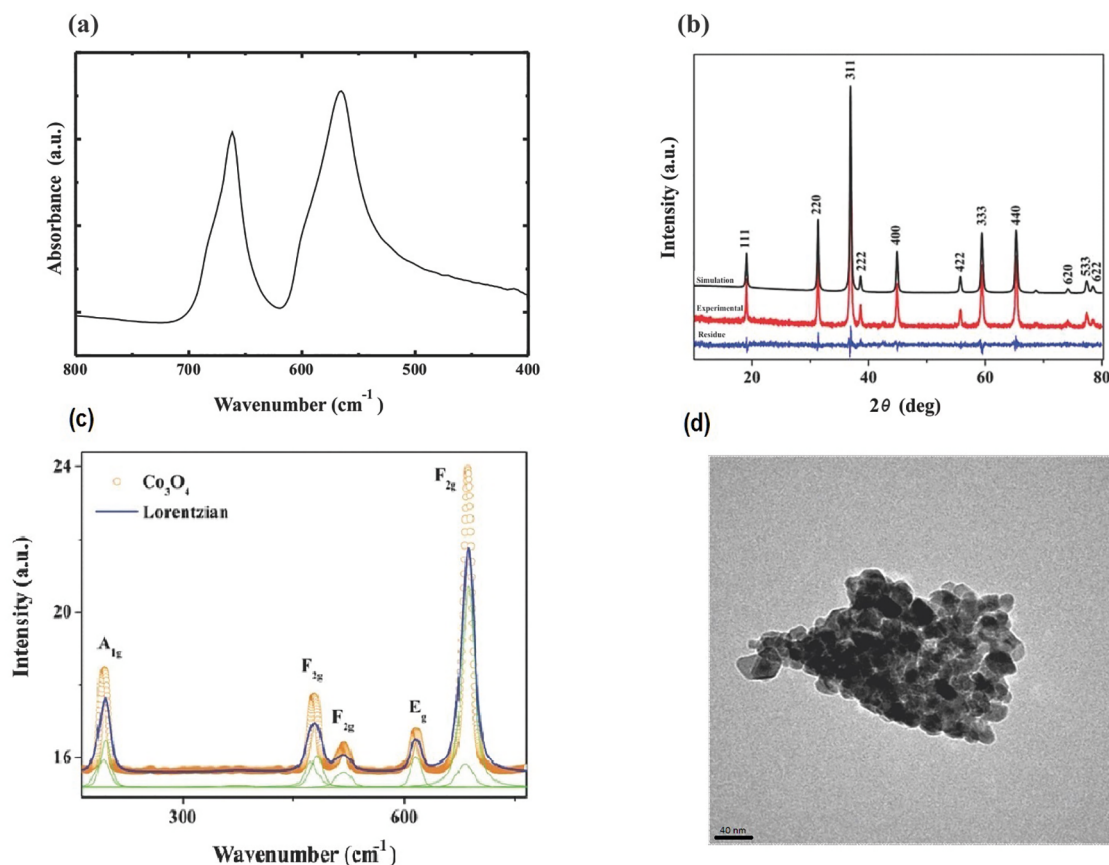


Figure 1. (a) FTIR spectrum of the synthesized Co_3O_4 nanoparticles. (b) XRD pattern for Co_3O_4 nanoparticles: simulation (Rietveld), experimental and residual lines (difference between experimental and simulated patterns). (c) Raman spectrum of Co_3O_4 nanoparticles. (d) TEM image of the Co_3O_4 nanoparticles

Fig. 1d shows a representative TEM image taken from Co_3O_4 nanoparticles. The image reveals undefined shape with similar particle size forming agglomerates that can be associated with the high surface energy of the nanometric crystals. The material synthesized when compared to other sol-gel methods, we can observe that the size of particles and agglomerates are similar, around 10 and 20 nm^{26,43}.

The voltammograms for the Co_3O_4 electrode at scan rates of 1, 25 and 100 mV s^{-1} in the potential range of 0 - 0.6 V for 1 mol L^{-1} KOH electrolyte is shown in Fig. 2a. It must be noted that the shapes of the curves are different from the shape presented by the electrical double layer capacitor which has closed rectangular shape and stored energy through non-faradaic processes⁴⁴. The voltammograms show forms that are typical of the materials that are strongly governed by faradaic processes with defined distinct anodic and cathodic peaks that represent the oxidation and reduction reactions occurring on the surface of Co_3O_4 electrode. The shape of the curves and the positions of the peaks (oxidation and reduction) in the voltammograms varied as a function of scan rate. The increase of scan rate caused a decrease in the definition and a displacement of those peaks. According to

Zhang⁴¹ the anodic peaks appear in the potential range of 0.4 to 0.6 V and represent the oxidation reactions of Co_3O_4 to CoOOH and CoOOH to CoO_2 . The cathodic peaks appear in the potential range of 0.3 to 0.5 V and represent the reduction reactions of CoO_2 to CoOOH and CoOOH to Co_3O_4 that are occurring on the surface of the electrode. To 25 mV s^{-1} scan rate the oxidation peak with a maximum at 0.55 V was broadest than the scan rate 1 mV s^{-1} , that was near 0.5 V. This suggests that a portion of material is not accessible when there is an increase of the scan rate, while lowest scan rate allows electrochemistry adsorption/desorption of the OH^- ions in the outer surface and inside the pores. On the other hand, the increase of scan rate allows access ions only on the external surface and, in this case, decreasing the storage charge values. According to Tummala²² the displacement of oxidation peaks to higher potentials and reduction peaks for lower potential may be related to conductivity and to the polarization of the electrode.

Fig. 2b shows the charge-discharge curves for current densities of 1, 3 and 5 mA cm^{-2} , at a potential range of 0 to 0.6 V in 1 mol L^{-1} KOH. In general, the shapes of the curves did not present good symmetry between the charge-discharge

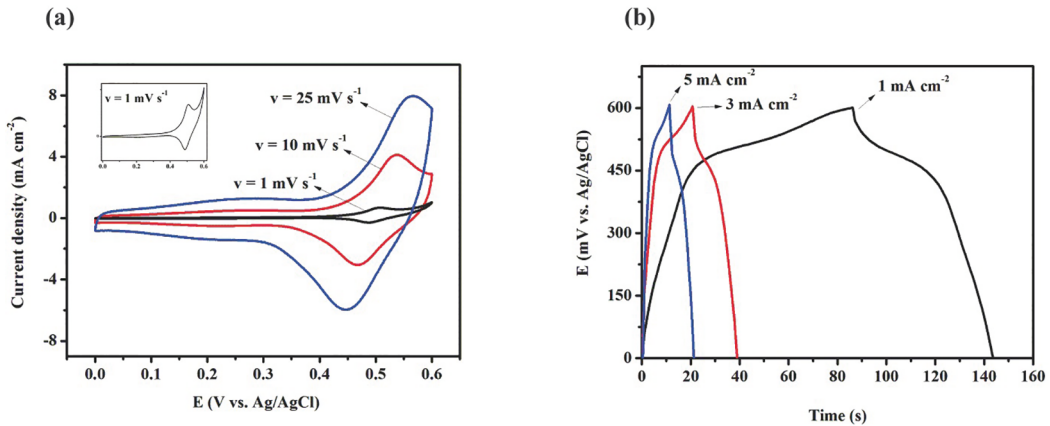


Figure 2. (a) Cyclic voltammograms at 1, 10 and 25 mV s^{-1} and (b) Charge-discharge at 1, 3 and 5 mA cm^{-2} at 1 mol L^{-1} of KOH for the Co_3O_4 nanoparticles

processes, and the curves were not ideally linear. A good symmetry may be related to a good reversibility of loading and unloading processes⁴⁵ and according to Vijayakumar¹⁴ nonlinearity is a confirmation of the pseudo-capacitive nature of the electrode. Discharge curves showed two distinct parts. Initially, the discharge curves show a resistive component which is represented by a rapid ohmic drop at the beginning of the discharge curve, it represents an internal resistance⁴⁶ and a capacitive part, represented by a potential decay over time at different inclinations due to Faradaic processes occurring in electrode surface⁴⁷. According to Lee⁴⁸ the rapid ohmic drop in potential is a characteristic of electrodes constituted by oxides of transition metals. The curves show that the increased current density favored the increase of the internal resistance. At low current density, the internal resistance is lower and allows a greater number of active sites utilized, which contributes to a higher stored energy.

The Nyquist plot, Fig. 3a, for the Co_3O_4 , and it is noted that high frequencies, where the curve intersects the real axis (axis Z'), have the electrolyte resistance (R_s) present values close to 0.4 Ω . The semicircle in the high frequency region corresponds to the charge transfer resistance (R_{ct}) due to faradaic reactions occurring at the electrode surface. The value R_{ct} to Co_3O_4 electrode is 3.6 Ω .

The imaginary part of the complex impedance Z'' in the region of least frequency provides information about the diffusive and capacitive processes. The straight line slope in the low frequency region for value close to 90° with respect to the axis Z' suggests that the capacitive behavior of Co_3O_4 electrode is not controlled by diffusion processes⁴⁹. The capacitive behavior was studied by the equation⁵⁰:

$$C(\omega) = \frac{1}{m\omega Z''(\omega)} \quad 1$$

where $\omega = 2\pi f$ is the angular frequency of the applied alternating current (ac) signal, m is the mass and Z'' is the imaginary part of the impedance. The behavior of capacitance

values with frequency from equation 1 is shown in Figure 3b. It was verified that for lowest frequency the capacitance maximum values obtained were of 120 F g^{-1} .

The data of electrochemical impedance spectroscopy were used at the study of complex capacitance to get the information of the relaxation time constant T_0 that represents the transition from resistive to the capacitive behavior⁵¹. The complex capacitance is expressed by the equation^{52,53}

$$C(\omega) = C'(\omega) - jC''(\omega) \quad 2$$

where j is imaginary number while the angular frequency is ω . $C'(\omega)$ e $C''(\omega)$ are the real and imaginary part of the complex capacitance $C(\omega)$ calculated by the following equations:

$$C'(\omega) = -\frac{z''(\omega)}{\omega |Z(\omega)|^2} \quad 3$$

$$C''(\omega) = \frac{z'(\omega)}{\omega |Z(\omega)|^2} \quad 4$$

where $|Z(\omega)|$ is the module of the complex impedance calculated by $Z(\omega) = Z'(\omega) - jZ''(\omega)$.

Figure 3c shows the imaginary part of the complex capacitance $C''(\omega)$ as a function of frequency for the studied concentration. The information of the relaxation time constant $T_0 = f_0^{-1}$ ^{49,50} was obtained by a maximum in frequency in f_0 . For frequencies $f > f_0$ the electrode presents the behavior of the resistor and for frequencies $f < f_0$ the electrode presents the behavior of the capacitor. Material that presents small values for the relaxation time constant exhibits rapid power delivery and provide high power density⁵⁴. The Co_3O_4 electrode presented a relaxation time constant about 20 s. Considering the frequency range used, the relaxation time constant varies from 0 to 100 s. The value obtained shows that during 20 s the electrode presented the behavior of the resistor and the time remaining presented the behavior of the capacitor.

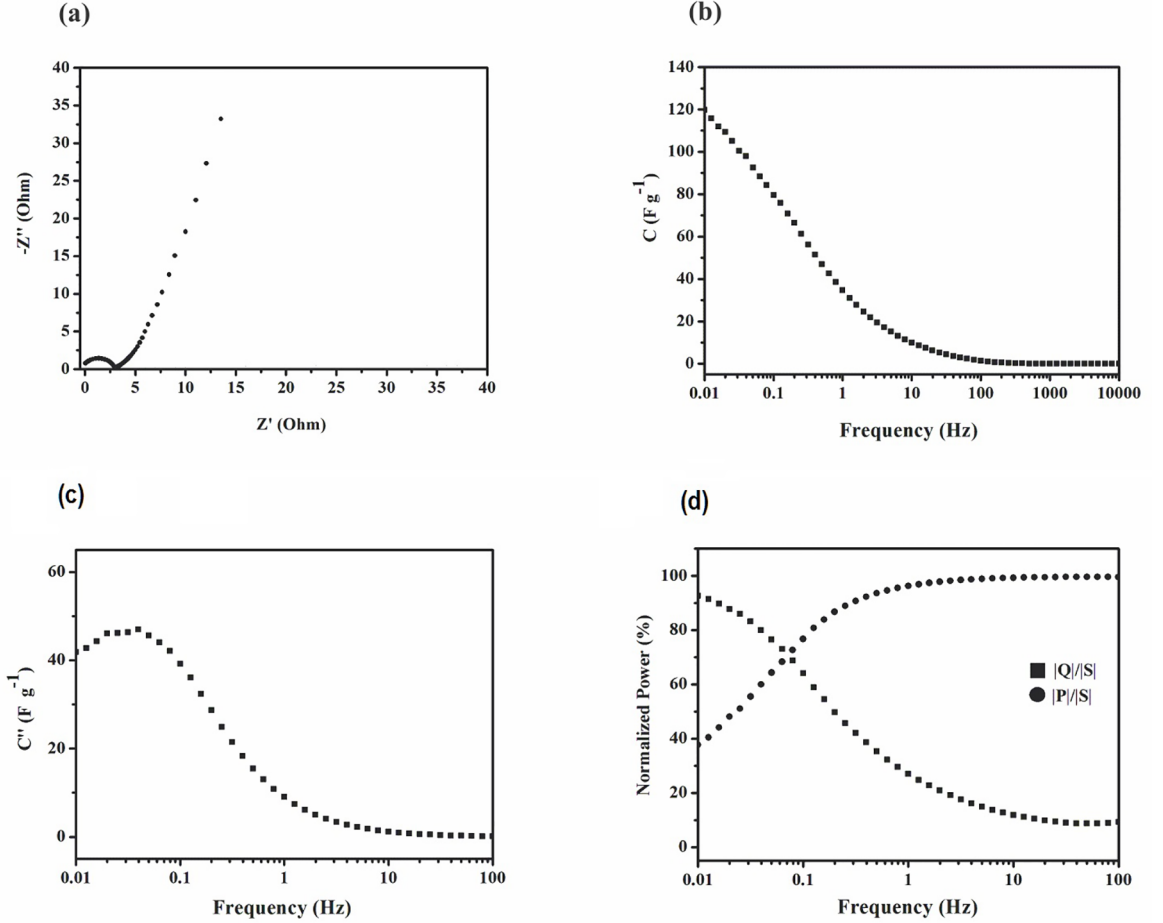


Figure 3. (a) Electrochemical impedance spectra for the Co₃O₄ nanoparticles and (b) Behavior of the specific capacitance as a function of frequency for the Co₃O₄ nanoparticles at 1 mol L⁻¹ of KOH solution. (c) Imaginary part of the complex capacitance C'' as a function of frequency and (d) Normalized power as a function of frequency for the Co₃O₄ nanoparticles at 1 mol L⁻¹ of KOH solution

Another form to express the data of electrochemical impedance is the study of complex power that shows the behavior of the active power (dissipated power) and reactive power (capacitive power) with the frequency. The total energy in circuits of alternating perturbation is the sum of the energy stored and the energy transferred in one direction. The total power (S) associated with this energy can be expressed in the complex form as the sum of the real part, transferred power or active power (P), and the imaginary part, stored power or reactive power (Q), as follows⁵⁵:

$$S(\omega) = P(\omega) + jQ(\omega) \quad 5$$

where P is the active power and Q is the reactive power calculated by relations

$$P(\omega) = \omega C''(\omega) |\Delta V_{rms}|^2 \quad 6$$

$$Q(\omega) = \omega C'(\omega) |\Delta V_{rms}|^2 \quad 7$$

where $\Delta V_{rms} = \frac{\Delta V_{max}}{\sqrt{2}}$ and ΔV_{max} is the maximum amplitude of the applied ac perturbation.

The power dissipated was analyzed from the normalization of the active and reactive powers, $|P|/|S|$ and $|Q|/|S|$, respectively. When the normalized powers $|P|/|S|$ and $|Q|/|S|$ are on the same graph as a function of frequency (Fig. 3d) it is verified that the concentrations studied began to present a capacitive response for frequency below 10 Hz and below 0.1 Hz showed a predominant capacitive behavior.

The set of the electrochemical tests indicate an intrinsic pseudocapacitance. The technique of cyclic voltammetry presented a curve with wide peaks and small peak-to-peak voltage separation (oxidation and reduction). The galvanostatic charge-discharge presented a curve with intermediate form of the forms presented by the materials used in batteries and capacitors. The impedance spectroscopy presented a curve containing a semicircle at high frequency followed by a straight line with a slope close to 90°^{10,56}.

4. Conclusion

Cobalt oxide nanoparticles Co_3O_4 were successfully prepared with an adapted sol-gel method. TEM images exhibit that the synthesized nanomaterial has no defined morphology. FTIR and DRX show the formation of nanoparticles Co_3O_4 spinel without the presence of secondary phases with the average size of the crystallites with about 30 nm. Raman Spectroscopy results confirm that observed peaks are characteristics of crystalline modes and consistent with the group theory for Co_3O_4 . The electrochemical tests revealed the characteristics of the resistive and capacitive behavior, showed an intrinsic pseudocapitance with specific capacitance of 120 F g^{-1} , which indicates that the method may be an option to obtain the cobalt oxide Co_3O_4 applied in the energy storage.

5. Acknowledgements

M.K.L is grateful to the CAPES for a doctorate fellowship. The authors also acknowledge financial assistance from FAPEAM (Grant #2985/2012).

6. References

- Ali AM, Najmy R. Structural, optical and photocatalytic properties of NiO-SiO₂ nanocomposites prepared by sol-gel technique. *Catalysis Today*. 2013;208:2-6.
- Wu ZY, Chen P, Wu QS, Yang LF, Pan Z, Wang Q. Co/Co₃O₄/C-N, a novel nanostructure and excellent catalytic system for the oxygen reduction reaction. *Nano Energy*. 2014;8:118-125.
- Hill AH, Harrison A, Ritter C, Yue W, Zhou W. Neutron powder diffraction and magnetic studies of mesoporous Co₃O₄. *Journal of Magnetism and Magnetic Materials*. 2011;323(2):226-231.
- Liu S, Wang Z, Zhao H, Fei T, Zhang T. Ordered mesoporous Co₃O₄ for high-performance toluene Sensing. *Sensors and Actuators B: Chemical*. 2014;197:342-349.
- Liu Y, Zhang X, Chang C, Zhang D, Wu Y. Promotive effect of multi-walled carbon nanotubes on Co₃O₄ nanosheets and their application in lithium-ion battery. *Progress in Natural Science: Materials International*. 2014;24(3):184-190.
- Wang X, Wang X, Liu L, Yi L, Hu C, Zhang X, et al. Synthesis and supercapacitive behavior of carbon aerogel microbeads encapsulated by in situ Co₃O₄ nanoparticle. *Synthetic Metals*. 2011;161(15-16):1725-1730.
- Cericola D, Kötz R. Hybridization of rechargeable batteries and electrochemical capacitors: Principles and limits. *Electrochimica Acta*. 2012;72:1-17.
- Zhou J, Li W, Zhang Z, Wu X, Xing W, Zhuo S. Effect of cation nature of zeolite on carbon replicas and their electrochemical capacitance. *Electrochimica Acta*. 2013;89:763-770.
- Conway BE. *Electrochemical Supercapacitors: Scientific Fundamentals and Technological Applications*. 1st ed. New York: Kluwer-Plenum; 1999.
- Augustyn C, Simon P, Dunn B. Pseudocapacitive oxide materials for high-rate electrochemical energy storage. *Energy & Environmental Science*. 2014;7(5):1597-1614.
- Come J, Augustyn V, Kim JW, Rozier P, Taberna PL, Gogotsi P, et al. Electrochemical kinetics of nanostructured Nb₂O₅ electrodes. *Journal of the Electrochemical Society*. 2014;161(5):A718-A725.
- Wang YG, Wang ZD, Xia YY. An asymmetric supercapacitor using RuO₂/TiO₂ nanotube composite and activated carbon electrodes. *Electrochimica Acta*. 2005;50(28):5641-5646.
- Li JL, Gao F, Jing Y, Miao RY, Wu KZ, Wang XD. Electrochemical characterization of MnO₂ as the cathode material for a high voltage hybrid capacitor. *International Journal of Minerals, Metallurgy and Materials*. 2009;16(5):576-580.
- Vijayakumar S, Nagamuthu S, Muralidharan G. Porous NiO/C Nanocomposites as Electrode Material for Electrochemical Supercapacitors. *Sustainable Chemistry & Engineering*. 2013;1(9):1110-1118.
- Nasibi M, Golozar MA, Rashed G. Nano iron oxide (Fe₂O₃)/carbon black electrodes for electrochemical capacitors. *Materials Letters*. 2012;85:40-43.
- Shan Y, Gao L. Formation and characterization of multi-walled carbon nanotubes/Co₃O₄ nanocomposites for supercapacitors. *Materials Chemistry and Physics*. 2007;103(2-3):206-210.
- Lang J, Yan X, Xue Q. Facile preparation and electrochemical characterization of cobalt oxide/multi-walled carbon nanotube composites for supercapacitors. *Journal of Power Sources*. 2011;196(18):7841-7846.
- Shinde VR, Mahadik SB, Gujar TP, Lokhande CD. Supercapacitive cobalt oxide (Co₃O₄) thin films by spray pyrolysis. *Applied Surface Science*. 2006;252(20):7487-7492.
- Balakrishnan A, Subramanian KRV, eds. *Nanostructured Ceramic Oxides for Supercapacitor Applications*. Boca Raton: CRC Press; 2014.
- Yan J, Wei T, Qiao W, Shao B, Zhao Q, Zhang L, et al. Rapid microwave-assisted synthesis of graphene nanosheet/Co₃O₄ composite for supercapacitors. *Electrochimica Acta*. 2010;55(23):6973-6978.
- Wang G, Shen X, Horvat J, Wang B, Liu H, Wexler D, et al. Hydrothermal Synthesis and Optical, Magnetic, and Supercapacitive Properties of Nanoporous Cobalt Oxide Nanorods. *Journal of Physical Chemistry C*. 2009;113(11):4357-4361.
- Tummala R, Guduru RK, Mohanty PS. Nanostructured Co₃O₄ electrodes for supercapacitor applications from plasma spray technique. *Journal of Power Sources*. 2012;209:44-51.
- Tototzintle-Huitle H, Prokhorov E, Mendoza-Galván A, Urbina JE, González-Hernández J. Study of the formation of Co₃O₄ thin films using sol-gel method. *Journal of Physics and Chemistry of Solids*. 2003;64(6):975-980.
- Drasovean R, Monteiro R, Fortunato E, Musat V. Optical properties of cobalt oxide films by a dipping sol-gel process. *Journal of Non-Crystalline Solids*. 2006;352(9-20):1479-1485.
- Armelaio L, Barreca D, Gross S, Martucci A, Tieto M, Tondello E. Cobalt oxide-based films: sol-gel synthesis and characterization. *Journal of Non-Crystalline Solids*. 2001;293-295:477-482.

26. Ivetić TB, Tadić M, Jagodić M, Gyergyek S, Štrbac GR, Lukić-Petrović SR. Structure and magnetic properties of Co₃O₄/SiO₂ nanocomposite synthesized using combustion assisted sol-gel method. *Ceramics International*. 2016;42(16):18312-18317.
27. Li Y, Wu H, Wu Y, Li Q. Facile synthesis of mesoporous Co₃O₄ nanowires for application in supercapacitors. *Journal of Materials Science: Materials in Electronics*. 2017;28(22):16826-16835.
28. Rosario AV, Bulhões LOS, Pereira EC. Investigation of pseudocapacitive properties of RuO₂ film electrodes prepared by polymeric precursor method. *Journal of Power Sources*. 2006;158(1):795-800.
29. Guo J, Chen L, Zhang X, Jiang B, Ma L. Sol-gel synthesis of mesoporous Co₃O₄ octahedra toward high-performance anodes for lithium-ion batteries. *Electrochimica Acta*. 2014;129:410-415.
30. Ferreira CS, Passos RR, Pocrifka LA. Synthesis and properties of ternary mixture of nickel/cobalt/tin oxides for supercapacitors. *Journal of Power Sources*. 2014;271:104-107.
31. Varshney P, Srinet G, Kumar R, Sajal V, Sharma SK, Knobel M, et al. Room temperature ferromagnetism in sol-gel prepared Co-doped ZnO. *Materials Science in Semiconductor Processing*. 2012;15(3):314-318.
32. Caglar Y. Sol-gel derived nanostructure undoped and cobalt doped ZnO: Structural, optical and electrical studies. *Journal of Alloys and Compounds*. 2013;560:181-188.
33. Kumar S, Chen CL, Dong CL, Ho YK, Lee JF, Chan TS, et al. Structural, optical, and magnetic characterization of Co and N co-doped ZnO nanopowders. *Journal of Materials Science*. 2013;48(6):2618-2623.
34. Fernandes DM, Silva R, Winkler Hechenleiner AAW, Radovanovic E, Melo MAC, Pineda EAG. Synthesis and characterization of ZnO, CuO and a mixed Zn and Cu oxide. *Materials Chemistry and Physics*. 2009;115(1):110-115.
35. Yu H, Tang Q, Wu J, Lin Y, Fan L, Huang M, et al. Using eggshell membrane as a separator in supercapacitor. *Journal of Power Sources*. 2012;206:463-468.
36. Chandrappa KG, Venkatesha TV. Generation of Co₃O₄ microparticles by solution combustion method and its Zn-Co₃O₄ composite thin films for corrosion protection. *Journal of Alloys and Compounds*. 2012;542:68-77.
37. Pudukudy M, Yaakob Z, Narayanan B, Gopalakrishnan A, Tasirin SM. Facile synthesis of bimodal mesoporous spinel Co₃O₄ nanomaterials and their structural properties. *Superlattices and Microstructures*. 2013;64:15-26.
38. Ma J, Zhang S, Liu W, Zhao Y. Facile preparation of Co₃O₄ nanocrystals via a solvothermal process directly from common Co₂O₃ powder. *Journal of Alloys and Compounds*. 2010;490(1-2):647-651.
39. ICSD. *Inorganic Crystal Structure Database*. Karlsruhe: Gmch-Institut für Anorganische Chemie und Fachinformationszentrum FIZ; 1995.
40. Louardi A, Rmili A, Ouachtari F, Bouaoud A, Elidrissi B, Erguig H. Characterization of cobalt oxide thin films prepared by a facile spray pyrolysis technique using perfume atomizer. *Journal of Alloys and Compounds*. 2001;509(37):9183-9189.
41. Hadjiev VG, Iliev MN, Vergilov IV. The Raman spectra of Co₃O₄. *Journal of Physics C: Solid State Physics*. 1988;21(7):L199.
42. Ai LH, Jiang J. Rapid synthesis of nanocrystalline Co₃O₄ by a microwave-assisted combustion method. *Powder Technology*. 2009;195(1):11-14.
43. Alizadeh-Gheshlaghi E, Shaabani B, Khodayari A, Azizian-Kalanderagh Y, Rahimi R. Investigation of the catalytic activity of nano-sized CuO, Co₃O₄ and CuCo₂O₄ powders on thermal decomposition of ammonium perchlorate. *Powder Technology*. 2012;217:330-339.
44. Zhang C, Xie L, Song W, Wang J, Sun G, Li K. Electrochemical performance of asymmetric supercapacitor based on Co₃O₄/AC materials. *Journal of Electroanalytical Chemistry*. 2013;706:1-6.
45. Liu MC, Kong LB, Lu C, Li XM, Luo YC, Kang L. Facile fabrication of CoMoO₄ nanorods as electrode material for electrochemical capacitors. *Materials Letters*. 2013;94:197-200.
46. Yang W, Gao Z, Ma J, Wang J, Wang B, Liu L. Effects of solvent on the morphology of nanostructured Co₃O₄ and its application for high-performance supercapacitors. *Electrochimica Acta*. 2013;112:378-385.
47. Jagdale AD, Dubal DP, Lokhande CD. Electrochemical behavior of potentiodynamically deposited cobalt oxyhydroxide (CoOOH) thin films for supercapacitor application. *Materials Research Bulletin*. 2012;47(3):672-676.
48. Lee DY, Yoon SJ, Shrestha NK, Lee SH, Ahn H, Han SH. Unusual energy storage and charge retention in Co-based metal-organic-frameworks. *Microporous and Mesoporous Materials*. 2012;153:163-165.
49. Wu JB, Lin Y, Xia XH, Xu JY, Shi QY. Pseudocapacitive properties of electrodeposited porous nanowall Co₃O₄ film. *Electrochimica Acta*. 2011;56(20):7163-7170.
50. Randriamahazaka H, Asaka K. Electromechanical Analysis by Means of Complex Capacitance of Bucky-Gel Actuators Based on Single-Walled Carbon Nanotubes and an Ionic Liquid. *Journal of Physical Chemistry C*. 2010;114(41):17982-17988.
51. Miller J. Pulse Power Performance of Electrochemical Capacitors: Technical Status of Present Commercial Devices. In: *Proceedings of the Eighth International Seminar on Double-Layer Capacitors and Similar Energy Storage Devices*; 1998 Dec 7-9; Deerfield Beach, FL, USA.
52. Taberna PL, Simon P, Fauvarque JF. Electrochemical Characteristics and Impedance Spectroscopy Studies of Carbon-Carbon Supercapacitors. *Journal of the Electrochemical Society*. 2003;150(3):A292-A300.
53. Yang C, Li CYV, Li F, Chan KY. Complex Impedance with Transmission Line Model and Complex Capacitance Analysis of Ion Transport and Accumulation in Hierarchical Core-Shell Porous Carbons. *Journal of the Electrochemical Society*. 2013;160(4):H271-H278.
54. Ganesh V, Pitchumani S, Lakshminarayanan V. New symmetric and asymmetric supercapacitors based on high surface area porous nickel and activated carbon. *Journal of Power Sources*. 2006;158(2):1523-1532.
55. Singh A, Chandra A. Significant Performance Enhancement in Asymmetric Supercapacitors based on Metal Oxides, Carbon nanotubes and Neutral Aqueous Electrolyte. *Scientific Reports*. 2015;5:15551.
56. Simon P, Gogotsi Y, Dunn B. Where Do Batteries End and Supercapacitors Begin? *Science*. 2014;343(6176):1210-1211.